CFD investigations of breaking focused wave-induced loads on a monopile and the effect of breaker location

Ankit Aggarwal *[1], Pietro D. Tomaselli[2], Erik Damgaard Christensen[2], and Hans Bihs[1]

[1]Department of Civil and Environmental Engineering, Norwegian University of Science and Technology (NTNU), 7491 Trondheim, Norway
[2]Fluid Mechanics, Coastal and Maritime Engineering, Department of Mechanical Engineering, Technical University of Denmark, Kgs. Lyngby, Denmark DK-2800

Journal of Offshore Mechanics and Arctic Engineering, 2020, **142** 2, pp. 021903.
DOI: http://dx.doi.org/10.1115/1.4045187

Abstract

The design of new offshore structures requires the calculation of the wave-induced loads. In this regard, the Computational Fluid Dynamics (CFD) methodology has shown to be a reliable tool, in the case of breaking waves especially. In this paper, two CFD models are tested in the reproduction of the experimental spilling waves impacting a circular cylinder for four different wave impact scenarios for focused waves. The numerical and experimental free surface elevations at different locations around the cylinder are also compared to verify both numerical models. The numerical results from the models are shown together with the experimental measurements. Both CFD models are able to model the impact forces with a reasonable accuracy. When the cylinder is placed at a distance of 0.7 m from the wave breaking point, the value of the measured wave impact forces is highest due to the overturning wave crest and air-entrainment. The wave-induced impact forces decrease, when the monopile is placed at distances further away from the breaking location.

Keywords: Computational Fluid Dynamics; REEF3D; focused wave; monopile; breaking wave; wave force

---

*Corresponding author,ankit.aggarwal@ntnu.no
Postprint, published in Journal of Offshore Mechanics and Arctic Engineering, doi:http://dx.doi.org/10.1115/1.4045187

1 Introduction

In designs of new offshore facilities, the evaluation of the structural stability crucially requires the analysis of the wave field at the site of interest and the determination of the wave-induced loads. Following the increasing trend of exploiting renewable energy sources, many new offshore structures will be wind turbines in the near future. As example, new Offshore Wind Farms are expected in the North-Sea between UK, the Netherlands, Germany and Denmark.

Most of these new offshore wind turbines will be built in intermediate water depth regions (20-60 m) where waves might break under storm conditions. The load exerted on a structure by a breaking wave can be different compared to non-breaking, possibly being much more severe Kjeldsen et al. (1986). In fact, the wave front becomes a mixture of water and air, changing the dynamics of the impact. The prediction of wave induced-loads on monopiles can be performed numerically. As example, the Morison equation Morison et al. (1950) has been widely used by designers. The Morison equation cannot be applied as such in the case of breaking waves and an additional empirical term is needed in order to account for the slamming effect Wienke and Oumeraci (2005); Hansen and Kofoed-Hansen (2017). The employment of the Computational Fluid Dynamics (CFD) methodology for predicting breaking wave-induced forces has gained much popularity recently, since it allows to reproduce the physics of the flow around the structure with a good approximation. The exerted forces can be computed by integrating the actual stresses on the surface of the structure Nielsen et al. (2008); Christensen et al. (2009); Bredmose and Jacobsen (2010); Paulsen et al. (2014). Further, the different impact scenarios for breaking regular waves have been investigated in the previous studies to understand the effect of the breaker location during the breaking process for regular waves Kamath et al. (2016).

The aim of the present study is to verify and compare two different CFD models and to investigate the effect of breaker location on a monopile for breaking focused waves. The first model is built in Tomaselli and Christensen (2016) with a particular configuration of the libraries provided by the open-source package OpenFOAM (version 2.3.1) and it will be called *waveEuler* hereafter. The second one is the open-source REEF3D Bihs et al. (2016) . The comparison is based on the numerical reproduction of an experiment, conducted at the Technical University of Denmark, in which the force exerted by a focused breaking wave on a circular cylinder was measured. The following sections will describe two CFD models, the experimental setup and the comparison of two sets of numerical results against the experimental measurements.

2 Description of the models

2.1 *waveEuler*

This model was specifically designed for reproducing the whole breaking process, i.e. wave propagation, breaking-induced air entrainment and evolution of the entrained air bubble plume. The solver was developed by the means of the open-source CFD libraries of OpenFOAM (version 2.3.1). The model *waveEuler* treats a wave as a two-phase system composed of air and water. During the breaking process, this water-air system is characterized by a broad range of interfacial length scales which spans from the free surface (meters, at a lab-

oratory scale) down to the small entrained air bubbles (fractions of a millimeter, Deane and Stokes (2002)) as reported in Tomaselli and Christensen (2015). In order to handle such different interfacial morphologies in the same spatial discretisation, *waveEuler* relies on a *coupling* between the Volume-of-Fluid (VOF) algorithm with the Eulerian multiphase approach. The former is used for capturing the free surface, while the latter can handle the physics of the dispersed air bubbles.

The governing Navier-Stokes equations for each phase i (water, air above free surface, bubbles) were expressed as:

$$\frac{\partial(\alpha_i \rho_i)}{\partial t} + \nabla \cdot (\alpha_i \rho_i \mathbf{u_i}) = S_i \tag{1}$$

$$\frac{\partial(\alpha_i \rho_i \mathbf{u}_i)}{\partial t} + \nabla \cdot (\alpha_i \rho_i \mathbf{u}_i \otimes \mathbf{u}_i) = -\alpha_i \nabla p + \nabla \cdot (\alpha_i \rho_i \mathbf{T}_i^{eff}) + \alpha_i \rho_i \mathbf{g} + \mathbf{M}_i \tag{2}$$

where t is the time, $0 \leq \alpha_i \leq 1$ is the void fraction, ρ_i the phase density, $\mathbf{g}$ the gravity acceleration, p is the pressure field assumed to be the same for all phases, and $\mathbf{u}_i$ the grid scale phase velocity. Closure formulations for the effective stress tensor $\mathbf{T}^{eff}$, for the momentum transfer $\mathbf{M}_i$ and the mass exchange S_i among bubbles were given in Tomaselli and Christensen (2016).

The governing equations (Eqs. 1-2) are discretised on collocated grids. The pressure-velocity coupling is handled by the PISO algorithm (Issa (1985)). The solver can be used for parallel computations by the means of the implemented MPI (Message Passing Interface) libraries.

In the present study, the two analysed CFD models were employed for reproducing the impact of a laboratory focused breaking wave on a cylinder located at four different locations with respect to the breaking point. The air entrainment module of *waveEuler* is not used in the present study, but will be applied in the future work. Applications of *waveEuler*, where the Eulerian multiphase approach was actually used in combination with the VOF algorithm can be found in Tomaselli and Christensen (2016) and Tomaselli and Christensen (2017).

2.2 REEF3D

The model is based on the governing equations of fluid dynamics: continuity equation and the Reynolds Averaged Navier-Stokes equations (RANS) with the assumption of an incompressible fluid given as:

$$\frac{\partial u_i}{\partial x_i} = 0 \tag{3}$$

$$\frac{\partial u_i}{\partial t} + u_j \frac{\partial u_i}{\partial x_j} = -\frac{1}{\rho}\frac{\partial p}{\partial x_i} + \frac{\partial}{\partial x_j}\left[(\nu + \nu_t)\left(\frac{\partial u_i}{\partial x_j} + \frac{\partial u_j}{\partial x_i}\right)\right] + g_i \tag{4}$$

where, u is the velocity averaged over time t, ρ is the fluid density, p is the pressure, ν is the kinematic viscosity, ν_t is the eddy viscosity, i and j denote the indices in x and y direction, respectively and g_i is the acceleration due to gravity.

The free surface is captured by the means of the level set method Osher and Sethian (1988). The level set function can be written as:

$$\phi(\vec{x},t)\begin{cases} > 0 & if\ \vec{x}\ is\ in\ phase\ 1 \\ = 0 & if\ \vec{x}\ is\ at\ the\ interface \\ < 0 & if\ \vec{x}\ is\ in\ phase\ 2 \end{cases} \tag{5}$$

A three-dimensional ghost cell immersed boundary method (GCIBM) Berthelsen and Faltinsen (2008) is implemented to model the complex geometries. Parallel computation is employed in the numerical model which is based on the domain decomposition method and MPI. The detailed information about the numerical model can be obtained in Bihs et al. (2016). REEF3D has been used in the past for a wide range of marine applications, such as breaking wave forces Aggarwal et al. (2019*a*,*b*), floating body dynamics Bihs and Kamath (2017), irregular wave analysis Aggarwal et al. (2018) and sediment transport Afzal et al. (2015).

3 The experiment

In the laboratory of the Technical University of Denmark, an experimental investigation was conducted on the impact of a focused breaking wave on a circular cylinder, chosen as representative of a real monopile structure. The test was carried out in a flume 28 m long by 0.60 m wide by 0.80 m high filled with water to a depth of $h_{sw} = 0.40$ and with a flat bottom. At the inlet, waves were produced by a piston-type wave generator provided with Active Wave Absorption Control System (AWACS) developed by DHI Water & Environment in order to avoid spurious reflection from the wavemaker. A system to absorb waves was also installed at the end of the flume.

The experimental setup is depicted in Figure 1. The cylinder was made of aluminum and had a diameter $D_{cyl} = 0.05$ m. Two force transducers measured the force at the bottom and the top. The total force was defined as the sum of these two contributions. A rail along the centerline of the bottom of the flume (x-axis) allowed to place the cylinder at different locations. The surface elevation was measured by the means of wave gauges (WG) at four stations: WG1 at 9.90 m from the inlet of the flume, and WG2, WG3, WG4 at -0.25 m, +0.0, +0.25 m from the cylinder respectively.

The experiment consisted of generating a wave train from still water conditions and of measuring the surface elevation at the four gauges and the forces on the cylinder (bottom and top) simultaneously. The wave train was derived from a JONSWAP spectrum ($T_p = 1.7$ s, $H_s = 0.084$ m, $\gamma = 3.3$) through the dispersive focusing technique. The JONSWAP spectrum was discretized in 80 linear components which were superposed such that the wave train produced a single spilling breaker at 11.20 m from the wave generator ($x_{br,exp} = 11.20$ m). The height $H_{br,exp}$ of the spilling breaker was estimated to be 0.22 m. The period $T_{br,exp}$ was 1.80 s.

With the same generated wave train, the experiment was repeated for different locations of the cylinder, which was moved at different distances $\hat{x}$ with respect to the fixed wave breaking point $x_{br,exp}$. Wave gauges WG2, WG3 and WG4 were moved as well, whereas WG1 was kept at 9.90 m from the inlet in each test. In the present study, four impact scenarios including the cylinder was placed at the wave breaking point ($\hat{x} = 0$ m, case A), cylinder placed at $\hat{x} =$ 0.7 m (case B), cylinder placed at $\hat{x} = 1$ m (case C) and cylinder placed at $\hat{x} = 1.5$ m (case D) were reproduced by the two CFD solvers. The list of simulation cases can be seen in Table 1. The comparisons of the experimental and numerical free surface elevations is presented for case A and case C for WG1, WG2, WG3 and WG4.

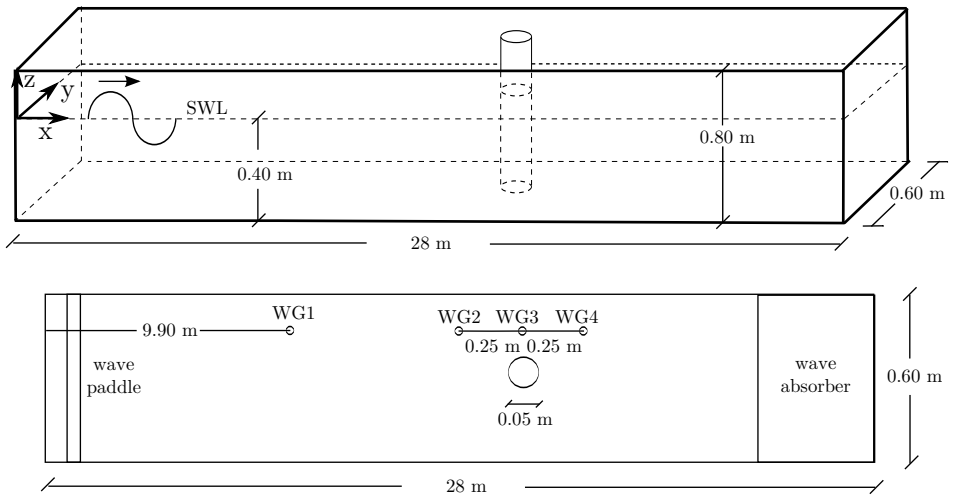

Figure 1: Sketch of the laboratory wave flume where the experiment was conducted; top: 3D view. bottom: view from above Tomaselli and Christensen (2017)

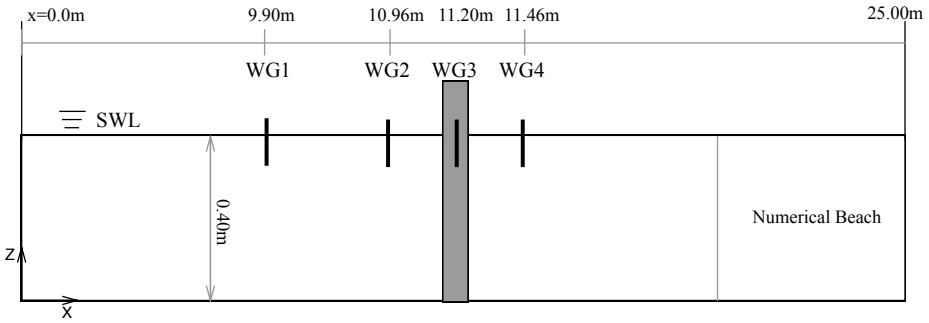

Figure 2: computational domain wave gauge locations for the simulations with REEF3D (side view)

4 Numerical Simulations

4.1 Simulation Setup

The extension of the computational domain was the same for both models, that is a numerical wave tank 25.0 m long by 0.60 m wide by 0.6 m high. A sketch of the domain for the simulations with REEF3D is given in Fig. 2. A similar one was used for *waveEuler*, but it is remarked that REEF3D employed the immersed boundary method for the discretisation of the cylindrical structure.

The model *waveEuler* adopted the relaxation method of Jacobsen et al. (2012) for wave generation and absorption. A relaxation zone of 4 m (from the inlet) was used for generating the waves. An absorption zone of 4 m was used at the end of the domain. REEF3D used Dirichlet boundary condition to generate waves and the relaxation method to absorb them.

Table 1: List of simulation cases

case	$\hat{x}$ (m)
A	0
B	0.7
C	1.0
D	1.5

For both models, the numerical input wave signal was reconstructed from the experimental paddle displacement. In fact, the reconstruction consisted of deriving the linear components to be superposed not from the JONSWAP spectrum illustrated in the previous section, but through the application of a Fourier transform algorithm on the experimental time series.

For the simulation with *waveEuler*, the mesh was structured with 4.6 million hexaedral cells with a size of 0.0125 m. The choice of this grid size was argumented in Tomaselli and Christensen (2017), where the same simulation was performed with the inclusion of entrained air bubbles. The size was a compromise between the computational demand, the accuracy of results and the constraint posed by Eulerian multiphase approach that the cell size must be larger than the bubble diameter. The cylinder was actually placed at $x = 12.65$ m, where the numerical wave breaking was observed to happen. The reasons for placing cylinder at 12.65 m in the waveEuler model were: (1) main reason could be the smearing of the interface due to VOF-advection with low order scheme which can affect the recognition of the breaking point; (2) wave generation method (relaxation zone) that could have affected the occurrence of breaking to a little extent. This was done in order to make a consistent comparison with the experimental measurements which were taken for the cylinder located at the wave breaking point ($\hat{x} = 0$). Wave gauges WG2, WG3 and WG4 were shifted accordingly. For waveEuler, the distances investigated in cases A, B, C and D are from the breaking point at 12.65 m.

A grid convergence study was carried out for REEF3D for case A. The placement of the cylinder in the REEF3D case is the same with the experiments at x=11.2. Three structured meshes with grid size $\Delta x = 0.05$ m, 0.025 m and 0.0125 m were tested. Figure 3 presents the comparison of experimental and simulated wave free surface elevation η with the different grid sizes at WG1, WG2, WG3 and WG4. At WG1, the numerical results with $\Delta x = 0.05$ m and 0.025 m showed slight errors in the numerical peak wave crest value as compared to the experimental value. The results for $\Delta x = 0.0125$ m showed a good agreement instead. At WG2, the experimental peak wave crest increased as the packet approached the energy focusing point. The results for $\Delta x = 0.05$ m and 0.025 m did not reproduce this circumstance satisfactorily (-24% and -14% respectively), while the simulation with $\Delta x = 0.0125$ m was in better agreement (-4.0%). At WG3, the laboratory waves focused further and they attained the maximum wave crest value. At this location, the most of the wave crest was observed to be vertical and it impacted the cylinder. The peak wave crest at WG3 was correctly represented only with the grid size $\Delta x = 0.0125$ m. After breaking, the experimental wave train dissipated some of the incident energy. The reduced peak wave crest measured at WG4 was well captured with the grid size $\Delta x = 0.0125$ m. Therefore, the best agreement between experimental measurements and numerical results was found for the simulation with a grid size $\Delta x = 0.0125$ m (3.5 million cells) as Table 2 highlights. This simulation was chosen for the comparison with the numerical results of *waveEuler* for which a similar grid size was used ($\Delta x = 0.0125$ m). The cell size in the vertical direction was 0.0125 m for both solvers.

Table 2: Grid convergence study for REEF3D; peak surface elevation value at the experimental wave gauges at different grid sizes for case A

	Grid size Δx [m]			Experiment [m]
	0.05	0.025	0.0125	
WG1	0.136	0.124	0.130	0.132
WG2	0.115	0.130	0.144	0.151
WG3	0.106	0.144	0.151	0.150
WG4	0.096	0.144	0.145	0.147

The model *waveEuler* employed the MULES algorithm for the convection of the phase fraction. Details about how this algorithm works can be found in Márquez Damián (2013). A scheme blending the first-order upwind and the second-order central differencing was adopted for the convective term of the momentum equation. The Euler implicit method was applied for the time discretization. The mesh was adjusted in each case to accommodate the cylinder (due to the body-fitted meshing). However, the mesh around the cylinder was the same in each case.

The model REEF3D used a fifth-order finite difference Weighted Essentially Non-Oscillatory (WENO) scheme in multi-space dimensions for the convection discretization of the flow velocities Shu (1997). The spatial discretization of the level set function is performed with the Hamilton-Jacobi version of the WENO scheme Jiang and Peng (2000). The third-order TVD Runge Kutta scheme was employed for the time discretization Shu and Gottlieb (1998). An adaptive time stepping scheme was used in both models Griebel et al. (1998). Time step was around 0.0040 s before breaking and 0.0005-0.001 s during breaking for both solvers. Both models employed turbulence closures. The $k-\omega$ model Wilcox (1994) and LES dynamics Smagorinsky model Germano et al. (1991); Lilly (1992) were used for REEF3D and *waveEuler* respectively. The force exerted on the cylinder was calculated by both solvers by integrating the pressure p and the wall shear stress τ acting over the surface of the structure at each time step. In this paper, only the in-line force F is reported and it can be given as

$$F(t) = \int_{-h_{sw}}^{\eta(t)} \left[\int_0^{2\pi} p \cos(\phi) \frac{D_{cyl}}{2} \, \mathrm{d}\phi + \int_0^{2\pi} \tau \sin(\phi) \frac{D_{cyl}}{2} \, \mathrm{d}\phi \right] \, \mathrm{d}z \tag{6}$$

where, ϕ is the angular coordinate.

The estimated values of Reynolds number *Re* and Keulegan-Carpenter *KC* indicated that the contribution from the shear stress was negligible and that the force was drag-dominated Sumer and Fredsøe (2006).

A flow of 35 seconds was covered by both models. The simulation with *waveEuler* took 20 hours on 40 cores of an HPC cluster, while REEF3D employed 6 hours on 512 cores.

4.2 Numerical results

The time-variation of the experimental and the numerical surface elevation simulated by the two solvers is presented for cases A and C in Figs. 4 and 5, respectively for WG1, WG2, WG3 and WG4.

Both solvers were in good agreement with the experiment, but REEF3D better reproduced the peak wave crest as Table 3 highlights for both cases A and C. Overall, both sets of

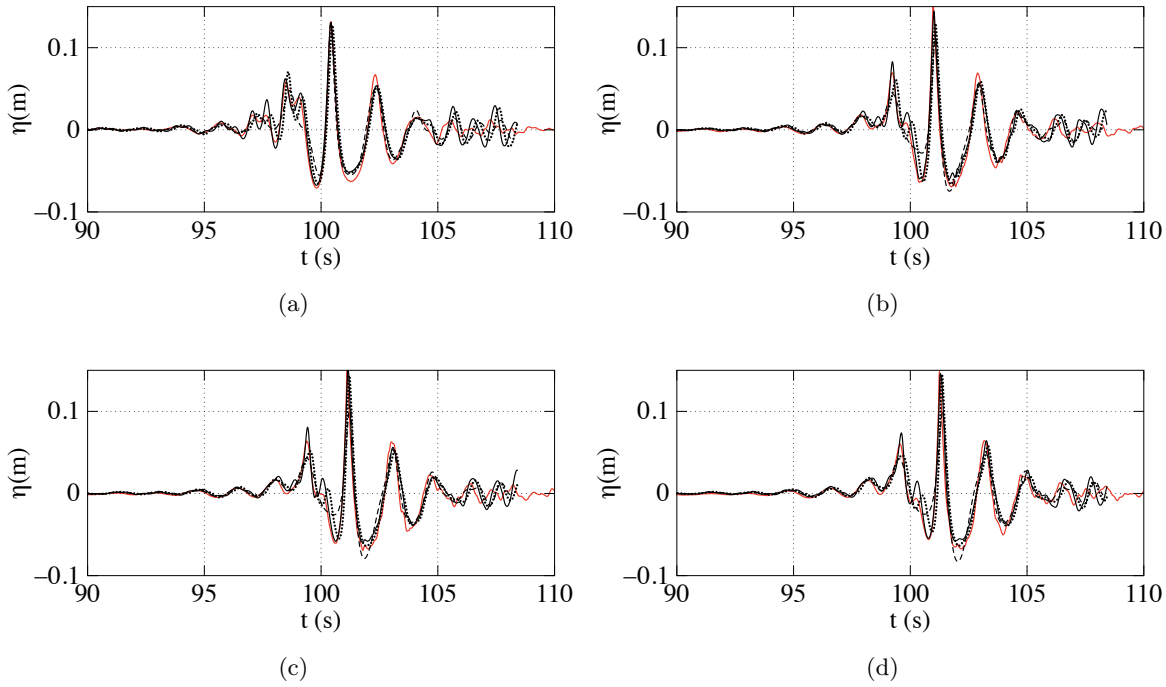

Figure 3: Experimental and numerical wave free surface elevation for case A at (a) WG1 (b) WG2 (c) WG3 (d) WG4. Red solid line presents experiments; black dashed line for Δx = 0.05m; black dotted line for Δx = 0.025m; black solid line for Δx = 0.0125m

numerical results suffered from some discrepancies at the crests and at the troughs of the wave train. The former could be attributed to the mesh resolution which is not high enough for the smaller waves of the train. The latter are likely due to the linear theory adopted for the wave generation procedure which neglected nonlinear interactions among the individual wave components. The experimental and the simulated in-line force on the cylinder are illustrated in Fig. 6 for all cases. In each case, the experimental time series showed a primary force peak which corresponded to the impact of the wave front at the breaking point. The wave breaking is followed by the generation of shorter waves with higher harmonics. These contributed to the secondary force peaks occurred after the wave breaking. Both models were able to reproduce the measured time-variation of the in-line force with a reasonable accuracy for each case, but they showed some disagreement in capturing the peak value.

For case A (Fig. 6a), when the cylinder is placed exactly at the breaking point ($\hat{x}$ = 0 m), REEF3D underestimated it (-12%), while *waveEuler* overestimated it (+17%). When the cylinder is placed at $\hat{x}$ = 0.7 m (case B), REEF3D and *waveEuler* models simulate this peak force with errors of -20 % and +36 %, respectively. For case C ($\hat{x}$ = 1 m), the error between REEF3D and the experimental peak force value reduces to -8%, while the error for *waveEuler* is +35% (Fig. 6c). The errors for REEF3D and *waveEuler* CFD models are +5% and +22%, respectively for case D (Fig. 6d). Table 4 and Fig. 7 summarize the results for peak force. It is clear from Fig. 7 that both the numerical models REEF3D and *waveEuler* model emulate the experimental trend of the peak wave force on moving the cylinder away

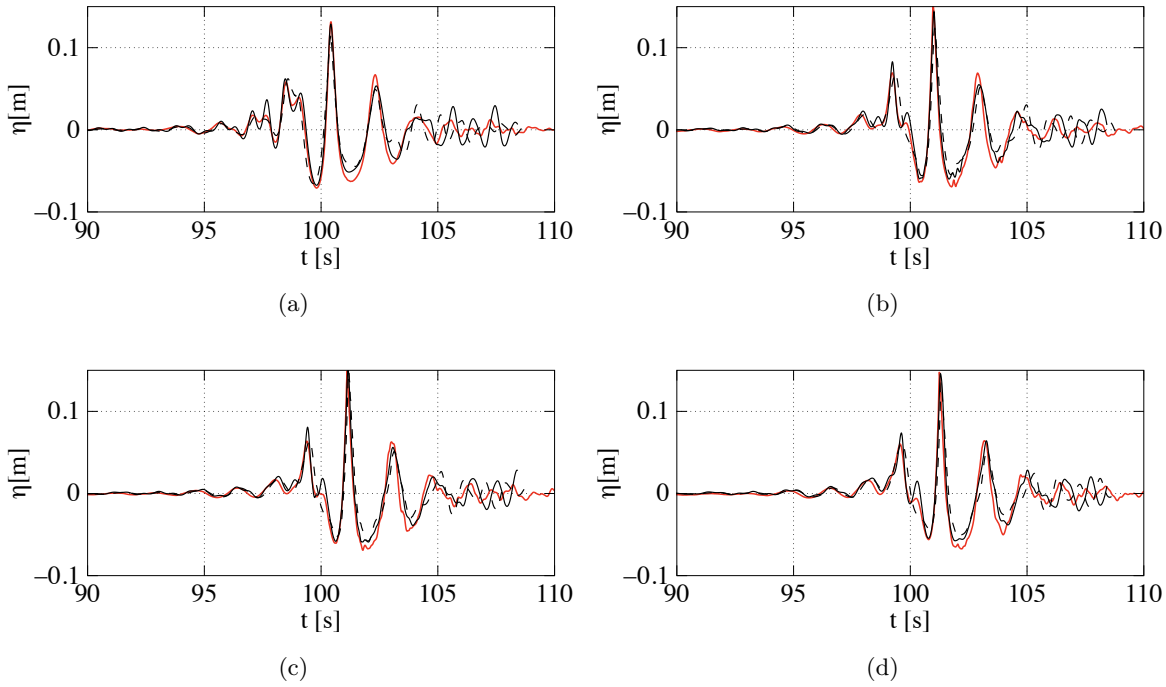

Figure 4: Comparison between *waveEuler* and REEF3D; time-variation of the experimental and simulated surface elevation for case A (a) WG1 (b) WG2 (c) WG3 (d) WG4. Red solid line presents experiments; black dashed line for *waveEuler*; black solid line for REEF3D

from the wave breaking location. In fact, the peak breaking wave force is measured when the cylinder is placed at $\hat{x} = 0.7$ m (case B). On further increasing the distance of the cylinder from breaking point, the value of peak wave forces decrease. The fact that the peak force was not maximum at breaking point, but slightly downstream might be related to the evolution of the air entrainment process and the overturning wave crest impacting the cylinder with a large mass of accelerating water. The errors shown by both models in the peak force was mainly attributed to the resolution of the mesh around the cylinder.

The estimated values of Re and KC indicated that the separation occurred in the boundary layer around the structure and that the vortex shedding regime established in the wake past the cylinder. The adopted mesh did not allow a detailed reconstruction of the boundary layer with a correct modelling of the separation points around the cylinder, especially at the top of the water column where the major contributions to the total force were exerted. For this circumstance, both solvers did not reproduce the correct pressure distribution around the cylinder. It is remarked that a higher mesh resolution, i.e. a smaller cell size, could not be used to refine the region around the cylinder. The reason was that the simulation with *waveEuler* employed the same mesh reported in Tomaselli and Christensen (2017), where the Eulerian multiphase approach prescribed the minimum cell size to be bigger than the diameter of the modelled entrained bubbles. On the other hand, the simulation with REEF3D used the same mesh resolution for consistency in the comparisons.

The differences in the results between REEF3D and *waveEuler* are believed to be due to the different numerical schemes adopted. REEF3D model is based on the higher-order

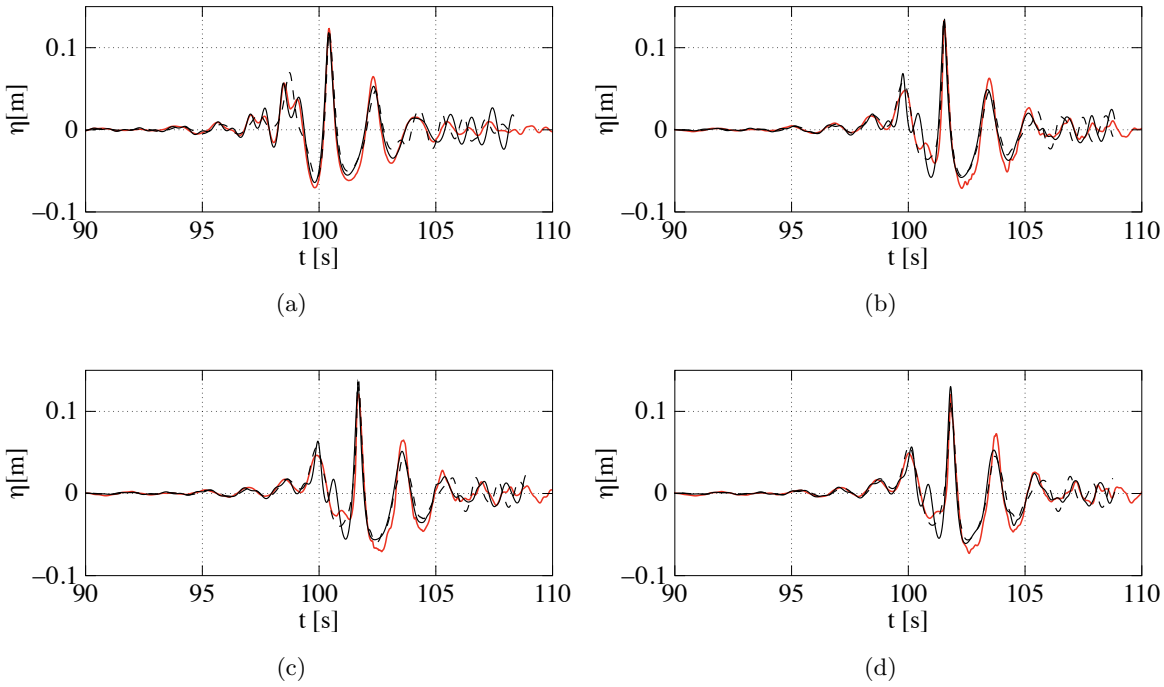

Figure 5: Comparison between *waveEuler* and REEF3D; time-variation of the experimental and simulated surface elevation for case C (a) WG1 (b) WG2 (c) WG3 (d) WG4. Red solid line presents experiments; black dashed line for *waveEuler*; black solid line for REEF3D

numerical schemes (Sec. 4.1), while *waveEuler* model is based on the relatively lower-order numerical schemes. The higher-order numerical schemes are able to represent the peak wave forces with a better accuracy compared to the lower-order numerical schemes at the same grid size. However, it should be kept in mind that solving the breaking wave force problem with the higher-order numerical schemes is relatively more expensive in terms of time. Another possible source of discrepancy between the two models is the wave generation method which is different (REEF3D generates waves by Dirichlet boundary condition and *waveEuler* uses the relaxation method). The different meshing approaches used in two solvers (body-fitted in *waveEuler* and immersed boundary method in REEF3D) might also contribute to discrepancies in the results.

Fig. 8 presents the normalised spectral force density versus frequency for cases A, B, C, and D. It is observed that the primary spectral force peak for case A is well reproduced at $f/f_p = 1$ with both the numerical models. However, none of the numerical models are able to reproduce the secondary and tertiary spectral force peaks in the higher-frequencies. For the case with cylinder at $\hat{x} = 0.7$ m (case B), both numerical and experimental spectral force density peaks are in a reasonable agreement. When the cylinder is placed further away from the breaking location ($\hat{x} = 1$ m, case C), the numerical model based on the higher-order numerical schemes (REEF3D) models the primary spectral force peak with an error of -7 % and the numerical model based on the lower-order numerical schemes (*waveEuler*) simulates the primary spectral force peak with an error of +10 %. For the case with cylinder at $\hat{x} = 1.5$ m (case D), both the numerical models slightly overestimate the primary spectral force peak and none of the numerical models capture secondary and tertiary force peaks in the higher

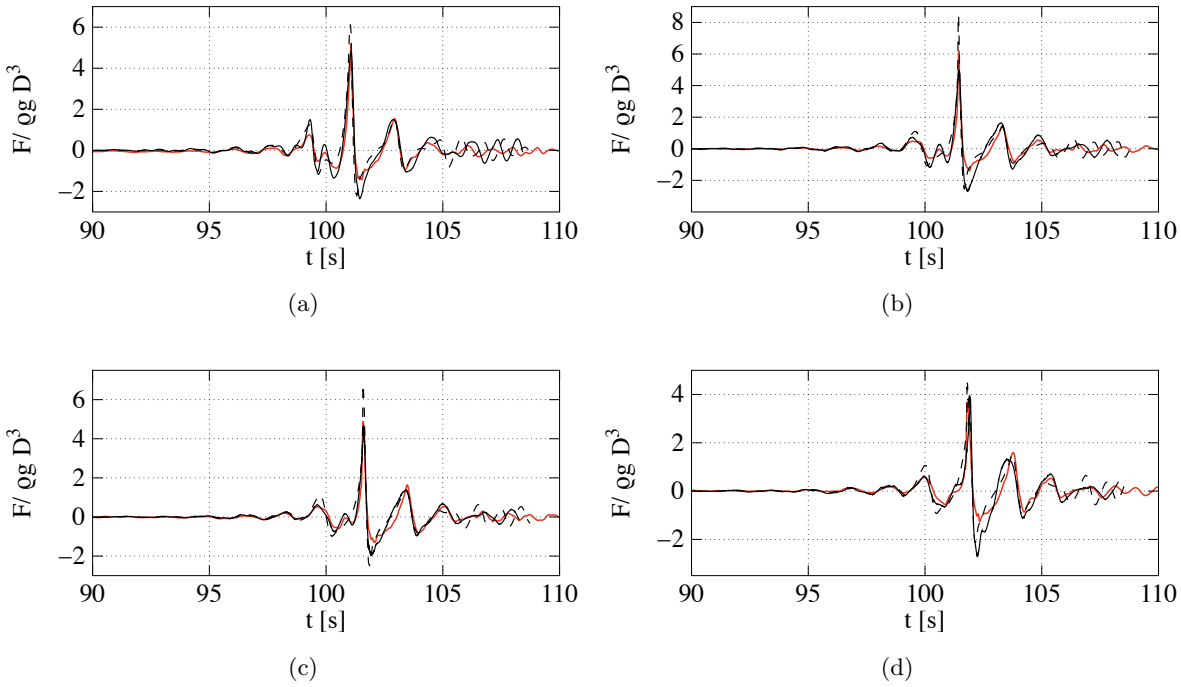

Figure 6: Comparison between *waveEuler* and REEF3D; time-variation of the experimental and simulated wave-induced force for (a) case A (b) case B (c) case C (d) case D. Red solid line presents experiments; black dashed line for *waveEuler*; black solid line for REEF3D

frequencies accurately.

In order to further investigate the breaking wave forces, rise time for the force peaks are analysed for the numerical and experimental data. Fig. 9 presents the the rise time of the peak forces versus the cylinder location with respect to the breaking point $\hat{x}$ for both CFD models and experiments. For all the cases A, B, C and D, the rise time of the wave impact loads on the cylinder is well represented in both the numerical models. For cases A and C, the rise time computed from REEF3D model is more close to the experimental value and for cases B and D, the rise time computed from *waveEuler* model is more close to the experimental rise time value.

5 Summary and Conclusions

The accurate computation of wave-induced loads is crucial in the design of new offshore structures. In this regard, numerical models based on the Computational Fluid Dynamics (CFD) methodology can be a very useful tool for designers, especially when waves are expected to break at the site of interest. The present study focused on a comparison of the results of two different CFD models which were employed to reproduce the same laboratory experiment. The experimental investigation, conducted at the Technical University of Denmark, consisted of a focused spilling wave impacting a cylinder which was placed at four distances with respect to the breaking point: 0 m, 0.7 m, 1 m, 1.5 m. The available measurements concerned the

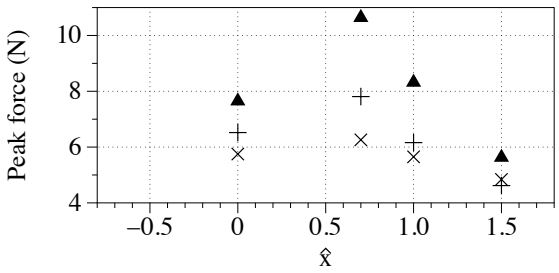

Figure 7: Comparison of numerical and experimental peak wave-induced forces versus $\hat{x}$; triangle is for *waveEuler*; plus for experiments; cross for REEF3D

Table 3: Comparison between *waveEuler* and REEF3D; peak surface elevation value at the experimental wave gauges

Case	WG	Numerical models (m)		Experiment (m)
		waveEuler	REEF3D	
A	WG1	0.126	0.130	0.132
	WG2	0.134	0.144	0.151
	WG3	0.150	0.151	0.150
	WG4	0.136	0.145	0.147
C	WG1	0.121	0.119	0.124
	WG2	0.137	0.132	0.133
	WG3	0.140	0.129	0.121
	WG4	0.113	0.129	0.121

Table 4: Comparison between *waveEuler* and REEF3D; peak in-line force exerted on the cylinder

Case	$\hat{x}$ (m)	Numerical models (N)		Experiment (N)
		waveEuler	REEF3D	
A	0	7.65	5.73	6.52
B	0.7	10.64	6.26	7.81
C	1	8.32	5.65	6.16
D	1.5	5.63	4.84	4.62

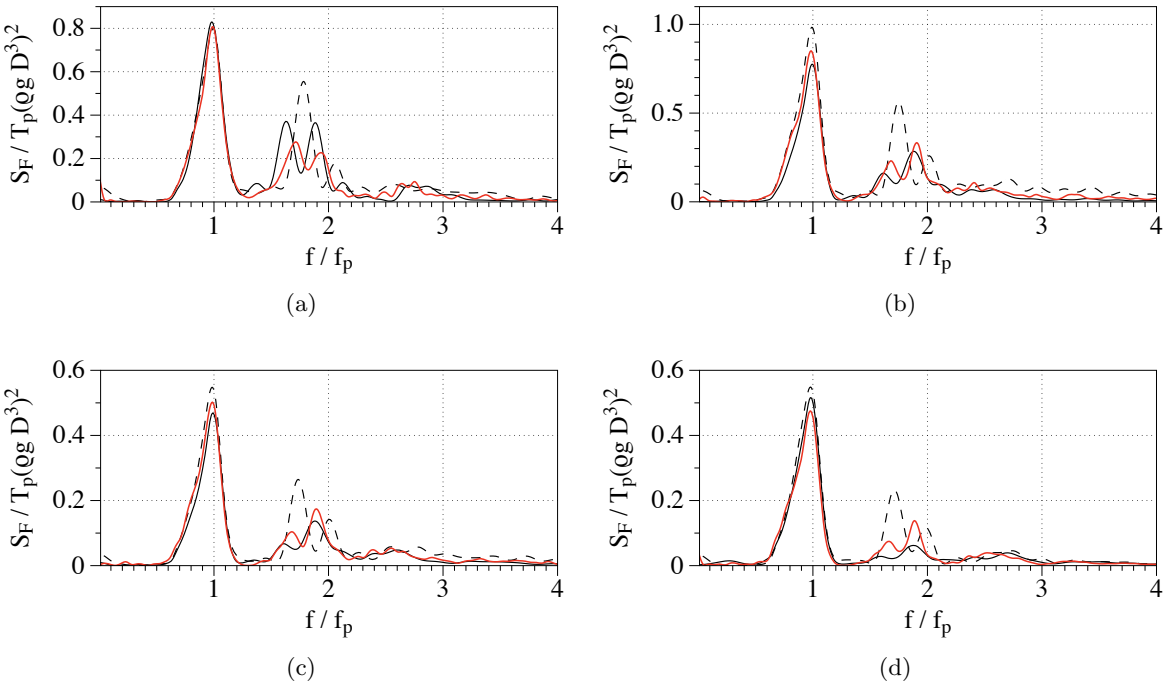

Figure 8: Comparison between *waveEuler* and REEF3D; frequency-variation of the experimental and simulated wave-induced force for (a) case A (b) case B (c) case C (c) case D. Red solid line presents experiments; black dashed line for *waveEuler*; black solid line for REEF3D

time-variation of the surface elevation (at four wave gauges) and of the in-line force exerted on the cylinder.

The two CFD models tested in this paper are *waveEuler*, a solver developed upon the open-source CFD package OpenFOAM, and REEF3D which is also open-source. Numerical simulations were conducted in a computational domain of the same extension. The mesh was structured in both cases, and same grid size was employed in both numerical models. The VOF-based solver *waveEuler* adopted a first-second-order blended scheme for the spatial discretization, a first-order scheme for the temporal discretization. The level-set-based model REEF3D employed a fifth-order scheme for the spatial discretization, a third-order scheme for the temporal discretization.

Both solvers reproduced the evolution of the free surface and of the force on the cylinder over time for all impact scenarios with reasonable accuracy. Moreover, both models emulated how the value of the peak force changed with increasing the distance of the cylinder with respect to breaking point (x). The peak force increased from x=0 and x=0.7, where the maximum is, and then decreased. The evolution of the air-entrainment during wave breaking process could be the possible reason of this behaviour that was observed both experimentally and numerically. In each impact scenario, the peak force caused by the impact of the breaking wave was not captured by either model with a great accuracy. Generally, *waveEuler* overestimated the peak, while REEF3D underestimated it. It was hypothesized that further increments of the grid resolution could improve the prediction of the peak force.

The performed comparison was an attempt to demonstrate the capabilities of two CFD

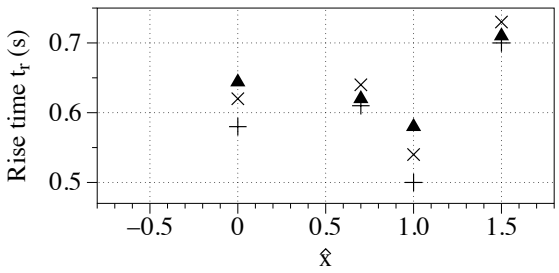

Figure 9: Comparison of numerical and experimental rise time for the peak wave-induced forces versus $\hat{x}$; triangle is for *waveEuler*; plus for experiments; cross for REEF3D

models with different characteristics and configurations. However, the numerical model based on higher-order numerical schemes (REEF3D) modelled the forces for these cases with a better accuracy, being closer to the experimental values. The numerical simulations with higher-order numerical schemes model the breaking wave forces more accurately compared to lower-order numerical schemes, but it should be kept in mind that the higher-order numerical schemes usually require relatively bit more computational time. In fact, waveEuler demanded 20 hours on 40 cores, while REEF3D employed 6 hours on 512 cores for each impact scenario.

In further studies, the role of air entrainment in determining the breaking wave forces will be investigated. The numerical results with REEF3D model will be compared with *waveEuler* model by using the air-entrainment module of the *waveEuler* and the recent improvements in OpenFOAM libraries Roenby et al. (2016) and configurations Larsen et al. (2017).

Acknowledgements

The research work related to REEF3D simulations has been funded by the Research Council of Norway through the project "Hydrodynamic Loads on Offshore Wind Turbine Sub- structures" (project number: 246810). The authors gratefully acknowledge the computing time granted by NOTUR (project number: NN2620K).

References

Afzal, M., Bihs, H., Kamath, A. and Arntsen. A., O. (2015). Three dimensional numerical modeling of pier scour under current and waves using level set method. *Journal of Offshore Mechanics and Arctic Engineering-Transactions of The Asme.*

Aggarwal, A., Alagan Chella, M., Bihs, H., Pákozdi, C., Petter, A. and Arntsen, O. (2018). Cfd based study of steep irregular waves for extreme wave spectra. *International Journal of Offshore and Polar Engineering*, **28(2)**, 164–170.

Aggarwal, A., Bihs, H., Alagan Chella, M. and Myrhaug, D. (2019*a*). Characteristics of breaking irregular wave forces on a monopile. *Applied Ocean Research*, **90**, 101846.

Aggarwal, A., Bihs, H., Alagan Chella, M. and Myrhaug, D. (2019*b*). Estimation of breaking wave properties and their interaction with a jacket structure. *Journal of Fluids and Structures*, **91**, 102722.

Berthelsen, P.A. and Faltinsen, O.M. (2008). A local directional ghost cell approach for incompressible viscous flow problems with irregular boundaries. *Journal of Computational Physics*, **227**, 4354–4397.

Bihs, H. and Kamath, A. (2017). A combined level set/ghost cell immersed boundary representation for simulations of floating bodies. *International Journal for Numerical Methods in Fluids*.

Bihs, H., Kamath, A., Alagan Chella, M., Aggarwal, A. and Arntsen. A., O. (2016). A new level set numerical wave tank with improved density interpolation for complex wave hydrodynamics. *Computers and fluids*, **140**, 191–208.

Bredmose, H. and Jacobsen, N.G. (2010). Breaking Wave Impacts on Offshore Wind Turbine Foundations: Focused Wave Groups and CFD. In: *Proceedings of the ASME 2010 29th International Conference on Ocean, Offshore and Arctic Engineering OMAE2010*.

Christensen, E.D., Bredmose, H. and Hansen, E.A. (2009). Transfer of Boussinesq Waves to a Navier-Stokes Solver: Application to Wave Loads on an Offshore Wind Turbine Foundation. In: *Proceedings of the ASME 2009 28th International Conference on Ocean, Offshore and Arctic Engineering*, 917–926. Honolulu, Hawaii. ISBN 0001424084.

Deane, G.B. and Stokes, M.D. (2002). Scale dependence of bubble creation mechanisms in breaking waves. *Nature*, **418**(6900), 839–44. ISSN 0028-0836. 10.1115/1.404518710.1038/nature00967.

Germano, M., Piomelli, U., Moin, P. and Cabot, W.H. (1991). A dynamic subgrid-scale eddy viscosity model. *Physics of Fluids A: Fluid Dynamics*, **3**(7), 1760. ISSN 08998213. 10.1115/1.404518710.1063/1.857955.

Griebel, M., Dornseifer, T. and Neunhoeffer, T. (1998). *Numerical Simulations in Fluid Dynamics*. SIAM.

Hansen, H.F. and Kofoed-Hansen, H. (2017). An engineering-model for extreme wave-induced loads on monopile foundations. In: *ASME 2017 36th International Conference on Ocean, Offshore and Arctic Engineering*, V03BT02A014. American Society of Mechanical Engineers.

Issa, R.I. (1985). Solution of the Implicitly Discretised Fluid Flow Equations by Operator-Splitting. *Journal of Computational Physics*, **62**, 40–65.

Jacobsen, N.G., Fuhrman, D.R. and Fredsøe, J. (2012). A wave generation toolbox for the open-source CFD library: OpenFoam. *International Journal for Numerical Methods in Fluids*, **70**, 1073–1088. 10.1115/1.404518710.1002/fld.

Jiang, G.S. and Peng, D. (2000). Weighted ENO schemes for Hamilton-Jacobi equations. *SIAM Journal of Scientific Computing*, **21**, 2126–2143.

Kamath, A., Alagan Chella, M., Bihs, H. and Arntsen, A., Ø. (2016). Breaking wave interaction with a vertical cylinder and the effect of breaker location. *Ocean Engineering*, **128**, 105–115.

Kjeldsen, S.r.P., Tørum, A. and Dean, R.G. (1986). Wave forces on vertical piles caused by 2 and 3 dimensional breaking waves. In: *Proceedings of the 20th International Conference on Coastal Engineering*, 1929–1942. Taipei. ISBN 978-1-4160-2591-7. 10.1115/1.4045187http://dx.doi.org/10.1016/B978-1-4160-2591-7.10142-0.

Larsen, B.E., Fuhrman, D.R. and Roenby, J. (2017). Performance of interfoam on the simulation of progressive waves. *Coastal Engineering*. Manuscript submitted for publication.

Lilly, D.K. (1992). A proposed modification of the Germano subgrid-scale closure method. *Physics of Fluids A: Fluid Dynamics*, **4**(3), 633. ISSN 08998213. 10.1115/1.404518710.1063/1.858280.

Márquez Damián, S. (2013). *An extended mixture model for the simultaneous treatment of short and long scale interfaces*. Ph.D. thesis, Universidad Nacional del Litoral, Argentina.

Morison, J., O'Brien, M., Johnson, J. and Schaaf, S. (1950). The Force Exerted by Surface Waves on Piles. *Journal of Petroleum Technology*, **AIME 189**, 149–154.

Nielsen, A.W., Mortensen, S.B., Jacoboson, V. and Christensen, E.D. (2008). Numerical modelling of wave run-up on a wind turbine foundation. In: *Proceedings of the ASME 27th International Conference on Offshore and Artic Engineering OMAE 2008*.

Osher, S. and Sethian, J.A. (1988). Fronts propagating with curvature- dependent speed: Algorithms based on Hamilton-Jacobi formulations. *Journal of Computational Physics*, **79**, 12–49.

Paulsen, B.T., Bredmose, H. and Bingham, H.B. (2014). An efficient domain decomposition strategy for wave loads on surface piercing circular cylinders. *Coastal Engineering*, **86**, 57–76. ISSN 03783839. 10.1115/1.404518710.1016/j.coastaleng.2014.01.006.

Roenby, J., Bredmose, H. and Jasak, H. (2016). A computational method for sharp interface advection. *Open Science*, **3**(11), 160405.

Shu, C. and Gottlieb, S. (1998). Total Variation Diminishing Range Kutta schemes. *Mathematics of Computation*, **67**, 73–85.

Shu, C.W. (1997). Essentially Non-Oscillatory andWeighted Essentially Non-Oscillatory Schemes for Hyperbolic Conservation Laws. Technical report.

Sumer, B.M. and Fredsøe, J. (2006). *Hydrodynamics around cylindrical structures*, volume 26. World Scientific. ISBN 9812700390.

Tomaselli, P.D. and Christensen, E.D. (2015). Investigation on the Use of a Multiphase Eulerian CFD Solver to Simulate Breaking Waves. In: *Proceedings of the ASME 2015 34th International Conference on Ocean, Offshore and Arctic Engineering*. St. John's, Newfoundland, Canada.

Tomaselli, P.D. and Christensen, E.D. (2016). A Coupled VOF-Eulerian Multiphase CFD Model to Simulate Breaking Wave Impacts on Offshore Structures. In: *Proceedings of the ASME 2016 35th International Conference on Ocean, Offshore and Arctic Engineering*. Busan, South Korea.

Tomaselli, P.D. and Christensen, E.D. (2017). A CFD investigation on the effect of the air entrainment in breaking wave impacts on mono-pile. In: *Proceedings of the ASME 2017 36th International Conference on Ocean, Offshore and Arctic Engineering*. Trondheim, Norway.

Wienke, J. and Oumeraci, H. (2005). Breaking wave impact force on a vertical and inclined slender pile—theoretical and large-scale model investigations. *Coastal Engineering*, **52**, 435–462. ISSN 03783839. 10.1115/1.404518710.1016/j.coastaleng.2004.12.008.

Wilcox, D. (1994). Turbulence modeling for CFD. *DCW Industries Inc. La Canada, California.*